Soil Science
Issue: Volume 162(11), November 1997, pp 771-777

Publication Type: [Article]
ISSN: 0038-075X
Accession: 00010694-199711000-00001

[Article]

NUMERICAL EVALUATION OF RING-INFILTROMETERS UNDER VARIOUS SOIL CONDITIONS

Wu, L.[1]; Pan, L.[1]; Roberson, M. J.[1]; Shouse, P. J.[2]

Author Information

[1]Department of Soil & Environmental Sciences, University of California, Riverside, CA92521. Dr. Laosheng Wu is corresponding author. E-mail: Laowu@mail.ucr.edu

[2]USDA/ARS, US Salinity Lab., Riverside, CA.
Received Feb. 24, 1997; accepted June 17, 1997.

Abstract

Field evaluation of infiltrometer geometry and of soil conditions on infiltration measurements is difficult because of the spatial and temporal variability of soil properties and the disturbance of soil by infiltrometer installation. Numerical simulation experiments provide a useful tool for evaluating the infiltration rates measured by various configurations of infiltrometers and soil conditions. We used an axisymmetric 3-dimensional (3-D) numerical model to simulate water infiltration in single- and doublering infiltrometers, as well as one-dimensional (1-D) infiltration for three well studied soil types representing different textures and hydraulic properties. We found that the infiltration rates of a single-ring infiltrometer were *f* times greater than the 1-D infiltration, where *f* is a correction factor dependent on soil initial and boundary conditions and ring geometry. When the configuration of a typical double-ring infiltrometer was used in simulation (inner and outer rings were 20 and 30 cm in diameter, respectively), the simulated infiltration rates were about 80% of the single-ring rates. When the outer-ring diameter was increased to 120 cm (inner-ring diameter kept at 20 cm), the double-ring method-measured infiltration rates were 120 to 133% of the 1-D infiltration rates for the three test soils. Compared with the constant head method, falling head infiltration rates dropped as much as 30% as the ponded head dropped from 5 to 1 cm in the sandy clay loam. Layered soil can significantly affect infiltration rates, depending on the position of the wetting front relative to the textural discontinuity and the time of measurement. Time at which the layering starts playing the role can be estimated from *f* and the cumulative infiltration.

Field water infiltration (or intake) rate at the soil surface is often measured using ring infiltrometers (Bouwer 1986). Measured infiltration rates depend on ring geometry, soil conditions, and time during the measurement sequence. Using an electrical resistance network analog and a piece-wise linear hydraulic conductivity function, Bouwer (1960) showed that the relative infiltration rate (i_f/K_s, where i_f is the final infiltration rate and K_s is saturated hydraulic conductivity) was dependent on the ratio of critical pressure, which is approximately one-half of the air-entry pressure value (Bower 1964; Fallow and Elrick 1996), to cylinder diameter. When a double-ring infiltrometer was used, Bouwer (1963) found that differences in water levels between the inner ring and buffer ring caused the erroneous infiltration rates measured in the inner ring.

Single-ring infiltrometers are probably the most widely used device for measuring field infiltration rates (Tricker 1978). In most vadose zone applications where infiltration information is used, the 1-D infiltration (vertical infiltration) capacity of the soil determines the rate at which water can be applied to the surface without runoff. Vertical infiltration is often described by the two-parameter Philip equation (Philip 1969). Infiltration from a ring-infiltrometer, however, is a 3-D problem (Philip 1966; Reynolds and Elrick 1990). Tricker (1978) divided the total infiltration capacity of a ring infiltrometer into two components: true (vertical) infiltration capacity and exaggerated infiltration capacity caused by lateral flow. A generalized relationship between 1-D (vertical infiltration capacity) and ring infiltrometers (total infiltration capacity) under various infiltrometer configurations is of great practical importance.

Using Gardner's (1958) hydraulic function and a shape factor accounting for various radii and insertion depths, Reynolds and Elrick (1990) developed a solution for steady-state water flow rate from a single-ring infiltrometer. Wu and Pan (1997) developed a generalized infiltration curve for single-ring infiltrometers by modifying the Reynolds and Elrick method to accommodate the popular van Genuchten (1980) hydraulic functions. Using a scaling technique, Wu and Pan (1997) applied their solution to soils with different initial and boundary conditions and found that the dimensionless infiltration curves were close to each other for their test soils. The characteristic infiltration rate (i_c) for a single-ring infiltrometer using their scaling technique is calculated by: Equation (1) and Equation (2) where Equation (3)-(6)

$$i_c = f K_s$$

Equation 1

$$f = \frac{H + \phi'_m / K_s}{G^*} + 1$$

Equation 2

$$G^* = d + r / 2$$

Equation 3

$$\phi'_m = \int_{hi}^{O} K'(h)\,dh$$

Equation 4

$$K'(h) = K_s \beta^{1/2m'} [1 - (1 - \beta)^{m'}]^2$$

Equation 5

$$\beta = [1 + (\alpha h)^n]^{-1} = Se^{1/m}$$

Equation 6

In Eqs. (1) to (6), d is ring insertion depth, r is the ring radius, and H is the ponding depth; $K(h)$ is hydraulic conductivity as a function of matric pressure h, h_i is the initial soil-water pressure head, S_e = ([theta] - $[\theta]_r$)/($[\theta]_s$ - $[\theta]_r$), and [alpha], n, m (m = 1 - 1/n) are coefficients in the van Genuchten (1980) water retention function. The modified van Genuchten hydraulic conductivity function, Eq. (5), was used with m' = 0.33; and $[\phi]_m'$ is the matric flux potential calculated by Eq. (4).

Infiltration rates are sometimes determined using hook or point gauges by measuring the time it takes for a water surface to drop a certain distance (Bouwer 1986). The solution of Elrick et al. (1995) can be used to evaluate the effects of falling head on infiltration rate measurements. In their approach, the steady-state solution to the ring infiltrometer problem is applied to the transient falling head conditions: Equation (7) with Equation (8) and Equation (9) where Q_s is the 'steady-state' flow rate ($L^3\ T^{-1}$). Q_s is related to the final infiltration rate, i_f ($L\ T^{-1}$), by dividing the cross-sectional area of the ring infiltrometer. The field-saturated hydraulic conductivity (K_{fs}) equals K_s in this study. Eq. (8) can be used to estimate the effect of falling head on the infiltration rate measurements.

$$Q_s = (r / G)(K_{fs}H(t) + \phi'_m) + \pi r^2 K_{fs}$$

Equation 7

$$H(t) = (H_0 + \phi'_m / K_{fs} + \pi r G)\exp(- rK_{fs}t / \pi r^2 G) - \phi'_m / K_{fs} - \pi r G$$

Equation 8

$$G = 0.316(d / r) + 0.184$$

Equation 9

In the field, evaluating the effects of soil conditions and ring geometry on infiltration measurements is difficult because of soil spatial variability and nonequal soil surface disturbance during ring installation. Such uncertainties make it impossible for the replicate field measurements needed to evaluate the effects of soil conditions and ring geometry on infiltration. Therefore, numerical evaluation (experiment) can be used as a tool to assess the effects of soil conditions and ring geometry on infiltration rates. The objectives of this research are to:

1. Evaluate infiltration rates numerically from single- and double-ring infiltrometers and 1-D infiltration
2. Assess the influence of constant- and falling-head methods on infiltration rates in various soils, and compare our numerical simulation with the infiltration rate calculated using Eq. (7)
3. Evaluate the effect of layering characteristics on infiltration rates.

MATERIALS AND METHODS

To simulate infiltration from ring infiltrometers, the axisymmetric form of the Richard equation was solved numerically using a finite difference method. Our model used a nonlinear transformed pressure as the dependent variable and a modified Picard method (Pan and Wierenga 1995, 1997), which improves the CPU efficiency and makes the model numerically robust under variably saturated conditions. van Genuchten [theta](h) and *K(h)* relationships with *m*' replaced by *m* = 1-1/n in Eqs. (5) and (6) were used for solving the Richards equation numerically.

Simulations were performed for 1-D infiltration, single-ring (*r* = 10 cm) infiltration, and a typical double-ring infiltrometer (the inner-ring *r* = 10 cm and outer-ring *r* = 15 cm; Bouwer 1986). Larger outer ring sizes (*r* = 20 cm and *r* = 60 cm) were also used to evaluate the effectiveness of larger outer ring size on reducing the lateral flow in the inner rings. The flow domain of our simulation was 100 cm by 100 cm. After completing each simulation, matric pressure and water content distributions in the flow domain were checked to make sure that the wetting front did not reach the boundaries. Boundary conditions were set to zero flux, except inside the rings, where constant head (*H* = 5 cm) or falling head conditions were prescribed. For the falling head simulation, the initial ponding head started at 5 cm. When the head fell to 1 cm, the model automatically "refilled" the infiltrometer to 5 cm. For numerical stability and CPU efficiency, various time and space steps were used for simulating infiltration in different soils. Initial soil-water pressure head was assumed to be -1000 cm. Simulated infiltration duration for the test soils varied according to their characteristic time (Wu and Pan 1997) and was slightly longer than the time required to reach 105% of the steady-state infiltration rate by Elrick et al. (1990).

Three well-studied soils representing different textures and hydraulic properties were chosen to conduct this research: the Berino fine sand (Hills et al. 1989), Yolo light clay (Warrick et al. 1985), and a sandy clay loam (Carsel and Parrish 1988). The hydraulic properties of the test soils are listed in Table 1.

Soil	θ_r (m^3m^{-3})	θ_s (m^3m^{-3})	α (cm^{-1})	n	K_s (cm min^{-1})
Berino fine sand	0.366	0.0286	0.028	2.34	0.3757
Sandy clay loam	0.390	0.100	0.059	1.48	0.02183
Yolo light clay	0.495	0.124	0.015	2.00	$7.3833e^{-4}$

TABLE 1 Hydraulic parameters in van Genuchten [theta](h) and $K(h)$ relationships of the test soils

RESULTS AND DISCUSSION

1-D, Single-Ring, and Double-Ring Infiltration

Figures 1a, 1b, and 1c show the simulated relative infiltration rates versus time for the Yolo light clay, the sandy clay loam, and the Berino fine sand for the cases of 1-D, single-, and double-ring infiltration. The infiltration rates from single- and double-ring and from 1-D infiltration were nearly identical, especially during the period before the wetting front advanced beyond the ring insertion depth, *d*. As time progressed, however, the infiltration rates for single- and double-ring infiltrometers and for 1-D infiltration diverged. Single-ring infiltrometers always had the highest final infiltration rate, followed by the double-ring and then the 1-D infiltration.

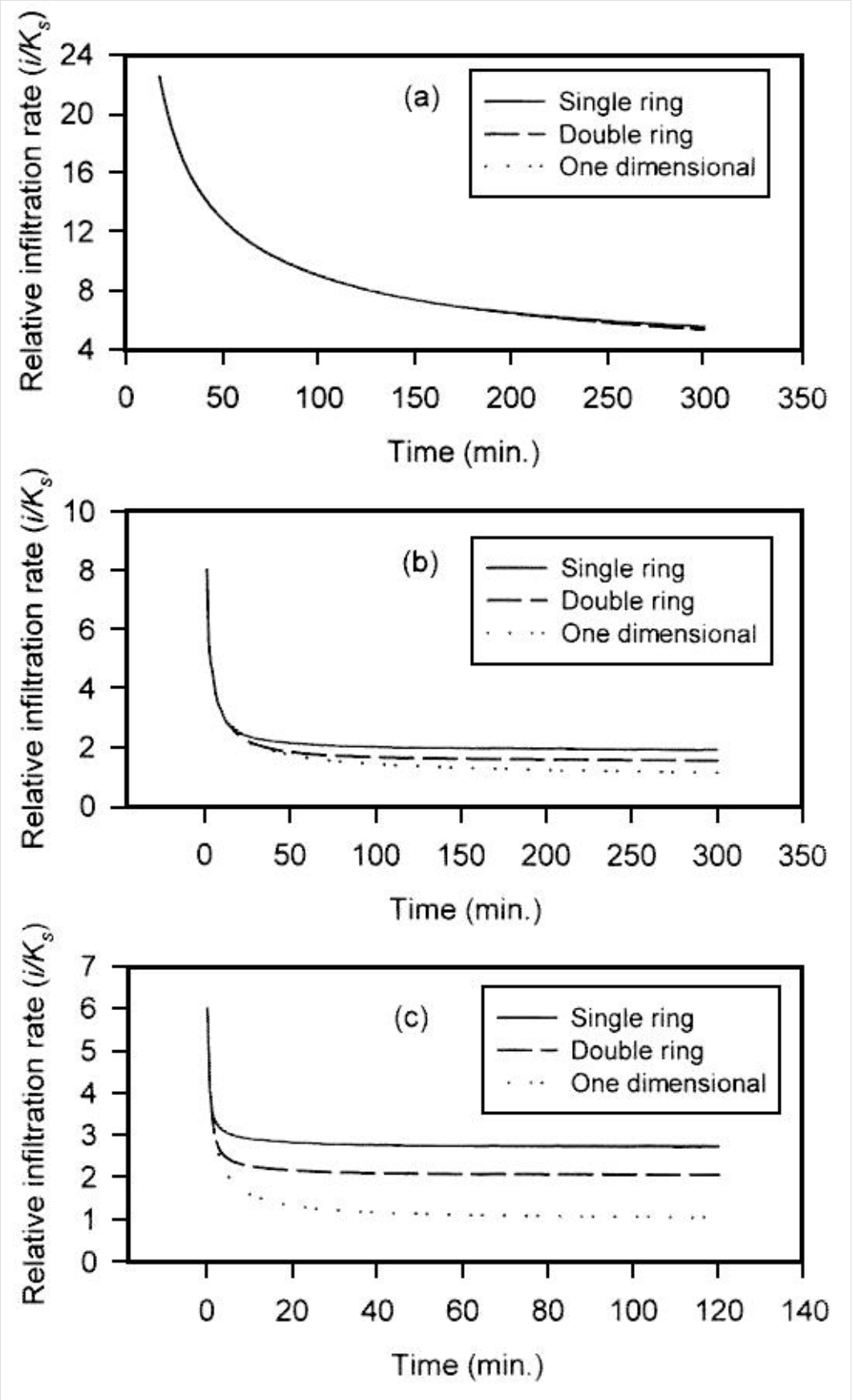

Fig. 1. Relative infiltration rate simulated for single-, double-ring, and 1-D cases for the Yolo light clay (a), sandy clay loam (b), and Berino fine sand (c) under constant head condition.

As soil texture becomes finer, the effect of ring configuration (diameter and insertion depth) becomes smaller for the early-time infiltration. This is because it takes a longer time for the wetting front to reach the depth of the ring insertion. For example, during the first 300 min. the differences among 1-D, single-, and double-ring infiltration were much greater in the sandy clay loam than in the Yolo light clay (Figs. 1a and 1b). It is expected, however, the differences in infiltration rates measured by the three methods would become larger in the Yolo light clay if a longer time period were used in the simulation.

Difference in final infiltration rates between 1-D and single-ring infiltration for the same soil can be related to the correction factor *f.* The *f* value relates infiltration rate (i_c) to the saturated hydraulic conductivity (K_s). For different ring radii (*r*) and insertion depths (*d*), the *f* values can be calculated from Eq. (2). It is clear that as *d* or *r* approaches infinity, the i_c approaches the steady-state 1-D infiltration rate (which equals K_s), because *G* approaches infinity and *f* approaches unity.

The *f* values are dependent on both soil initial and boundary conditions. Using the same initial soil water pressure of -1000 cm for each soil type, the resulting *f* values did not show a complete dependence on soil texture, but rather a dependence on the hydraulic conductivity function (Eq. (4)). The *f* values for the Berino fine sand, sandy clay loam, and Yolo light clay were 2.57, 1.87, and 3.29, respectively. This implies that the final infiltration rate does not depend completely on texture. This observation is different from the result of Bouwer (1960), who showed that the relative infiltration increased as the critical pressures increased when the same size ring were used, and finer soil usually has higher critical pressure. However, it is consistent with the results of Hanks and Bowers (1963). They showed that variations in soil-water diffusivity or water content near saturation had a strong influence on infiltration. The *f* values are also strongly affected by the hydraulic conductivity near saturation inasmuch as *f* is a function of $[phi]_m'$, and $[phi]_m'$ is the integration of *K(h)* over h. *K(h)* near saturation is usually several orders of magnitude greater than *K(h)* on the dry end of the curve. This observation agrees with Philip (1966), who found that the final steady-state infiltration rate depends both on hydraulic conductivity and the capillary properties of the soil.

Table 2 lists the final infiltration rates simulated for the 1-D infiltration and single- and double-ring infiltrometers. After the infiltration rates from the single-ring infiltrometer had been divided by the *f* values, they were very similar to the 1-D relative infiltration rate (unity). Because the relative infiltration rate was defined as infiltration rate divided by K_s, a unit final relative infiltration rate means that the final infiltration rate is equal to K_s of the soil. The relative infiltration rates from the single-ring infiltrometer, after being divided by *f* (*SR/ f*), were 1.08 for the Berino fine sand, 1.02 for the sandy clay loam, and 1.07 for the Yolo light clay. These values were very close to the 1-D relative infiltration rates of the three soils (1.00, 1.05, and 1.07, respectively). This implies that the method used in this study was effective. Wu and Pan (1997) found that the same approach could be applied to various ring sizes and soil initial and boundary conditions as well as various ponding depths.

Soil	1-D	SR	*f*	SR/*f*	DR1*	DR2	DR3
Berion fine sand	1.00	2.777	2.574	1.08	2.063	1.843	1.201
Sandy clay loam	1.05	1.914	1.869	1.02	1.557	1.475	1.200
Yolo light clay	1.07	3.516	3.287	1.07	2.495	2.177	1.331

*Double-ring infiltrometer with inner ring dia. of 0.2 m, and outer ring dia. of 0.3 (DR1), 0.4 (DR2), and 1.2 m (DR3).

TABLE 2 Relative infiltration rates (i_f/K_s) of 1-D, single- and double-ring infiltrometer and the correction factor (*f*)

When using a typical double-ring infiltrometer configuration (20-cm inner-and 30-cm outer-ring diameters), the simulated infiltration rates were about 80% of the infiltration rates of a single-ring infiltrometer and 56 to 150% higher than 1-D infiltration rates (Table 2). An outer-ring diameter of 40 cm did not substantially reduce the difference in infiltration rates between 1-D and double-ring infiltration. As the out-ring diameter increased to 120 cm, the double-ring infiltrometer measured infiltration rates were 20 to 33% higher than the 1-D infiltration rates (Table 2).

Constant versus Falling Head

The relative infiltration rates for the sandy clay loam using the constant and falling head methods were the same at the beginning of the simulation (Fig. 2a). As time progressed, the differences in the relative infiltration rates between constant head and falling head increased. This was the result of increased head difference between the two methods.

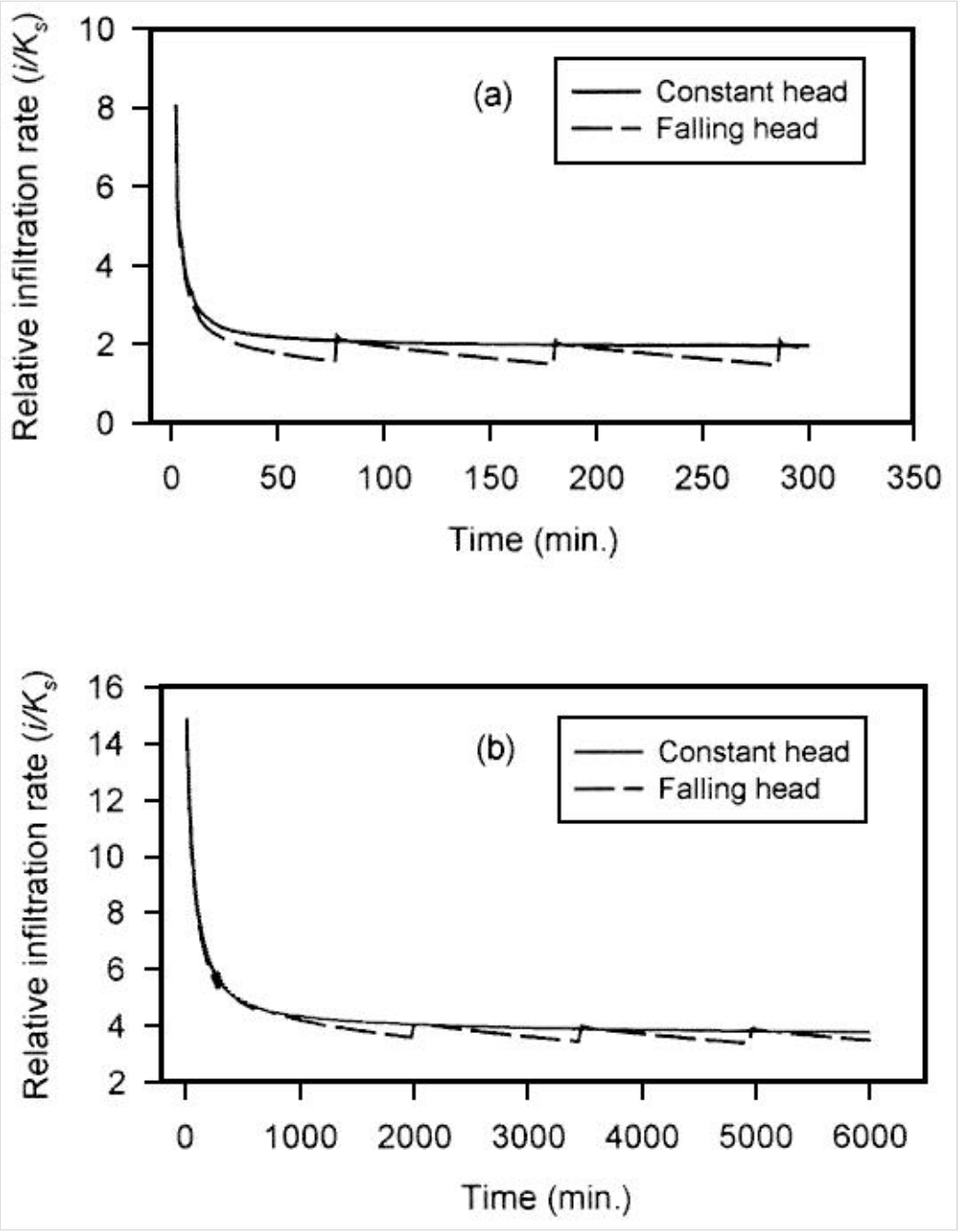

Fig. 2. Relative infiltration rate simulated for constant and falling head methods using a single-ring infiltrometer for the sandy clay loam (a) and Yolo light clay (b).

Figure 2b compares the relative infiltration rates of the constant and falling head methods for the Yolo light clay. As expected, both the constant and falling head started with the same infiltration rate, but the *i* dropped much faster for the falling head method than for the constant method. After the ring was refilled, the infiltration rate for the falling head method was brought back slightly higher than the *i* for the constant head method.

The numerically simulated infiltration rates at 5- and 1-cm ponded head after the last refill were compared with the steady-state infiltration rates calculated from Eq. (7) using the same heads. Table 3 lists the numerically simulated infiltration rates at 5- and 1-cm ponded heads, and the relative change in infiltration rate (%) when the ponded heads dropped from 5 to 1 cm. Using Eq. (8) resulted in a head drop from 5 to 1.27 cm for the sandy clay loam and from 5 to 1.76 cm for the Yolo light clay, whereas numerical simulation resulted in a head drop from 5 to 1.01 and 1.03 cm for these two soils. The relative infiltration rates at 5-cm ponded head from numerical simulation were 2.11 for the sandy clay loam and 4.02 for the Yolo light clay, compared with the calculated relative infiltration rates of 1.81 and 3.14 for the two soils. The final relative infiltration rates were 1.47 for the sandy clay loam and 3.36 for the Yolo light clay. These numbers reflect an infiltration rate decrease of 30.3 and 16.4% in numerical simulation, and 23.9 and 10.6% in solution of Elrick et al. (1995), respectively, for the sandy clay loam and Yolo light clay when the ponded head dropped from 5 to 1 cm. The difference can be attributed partially to the fact that steady-state has not been fully reached in the numerical simulation. In practice, however, the numerically simulated scenario is probably more likely to happen because field measurements seldom reach true steady state. However, solutions of Elrick et al. (1995) provide a good estimation of the difference between a constant head and a falling head method. It is obvious that the measured infiltration rate will depend on the timing of the measurement during a falling head infiltration process. However, if one measures infiltration rate right after the refilling, the measured infiltration rate will be very close to the constant head method (Fig. 2).

	Simulated						Elrick et al.					
Soil	H_0 cm	i_0	$t_s - t_0$ min.	H_s cm	i_s	$(i_s - i_0)/i_s$ %	H_0 cm	i'_0	$t_s - t_0$ min.	H'_s cm	i'_s	$(i'_s - i'_0)/i'_s$ (%)
Berino fine sand	5.0	2.72	4.0	1.15	2.33	14.3	5.0	2.47	4.0	1.54	2.14	15.0
Sandy clay loam	5.0	2.11	105.0	1.01	1.47	30.3	5.0	1.81	105.0	1.27	1.46	23.9
Yolo light clay	5.0	4.02	1470	1.03	3.36	16.4	5.0	3.14	1470	1.76	2.84	10.6

TABLE 3 Numerically simulated final relative infiltration rates and steady-state infiltration rate calculated by Eq. (8) for falling head method at t_0 ($H = H_0$) to t_s (H = 1 cm)

Effect of Layered Soil on Infiltration

The above simulation and discussion were based on homogeneous soil conditions. Layering due to agricultural practices and natural deposits is a common phenomenon in field soils. Infiltration rates measured at the soil surface in a layered soil will be different from those measured in a homogeneous soil. Figure 3a shows the relative infiltration rates versus time for the Berino fine sand with a uniform soil profile (single layer) and for the Berino fine sand overlaid on the sandy clay loam at 15, 20, and 30 cm under a single ring with constant head infiltration. The Figure shows that the final infiltration rate was affected by the position of the texture discontinuity. For the same measurement duration, the final infiltration rate in a layered soil differed most from the uniform soil when the underlain soil was close to the surface. For the case of the sandy clay loam overlaid on the Yolo light clay, the layering effect on infiltration was minimal for the first 300 min. (Fig. 3b). It is expected that the layering effect will become more substantial for a longer simulation.

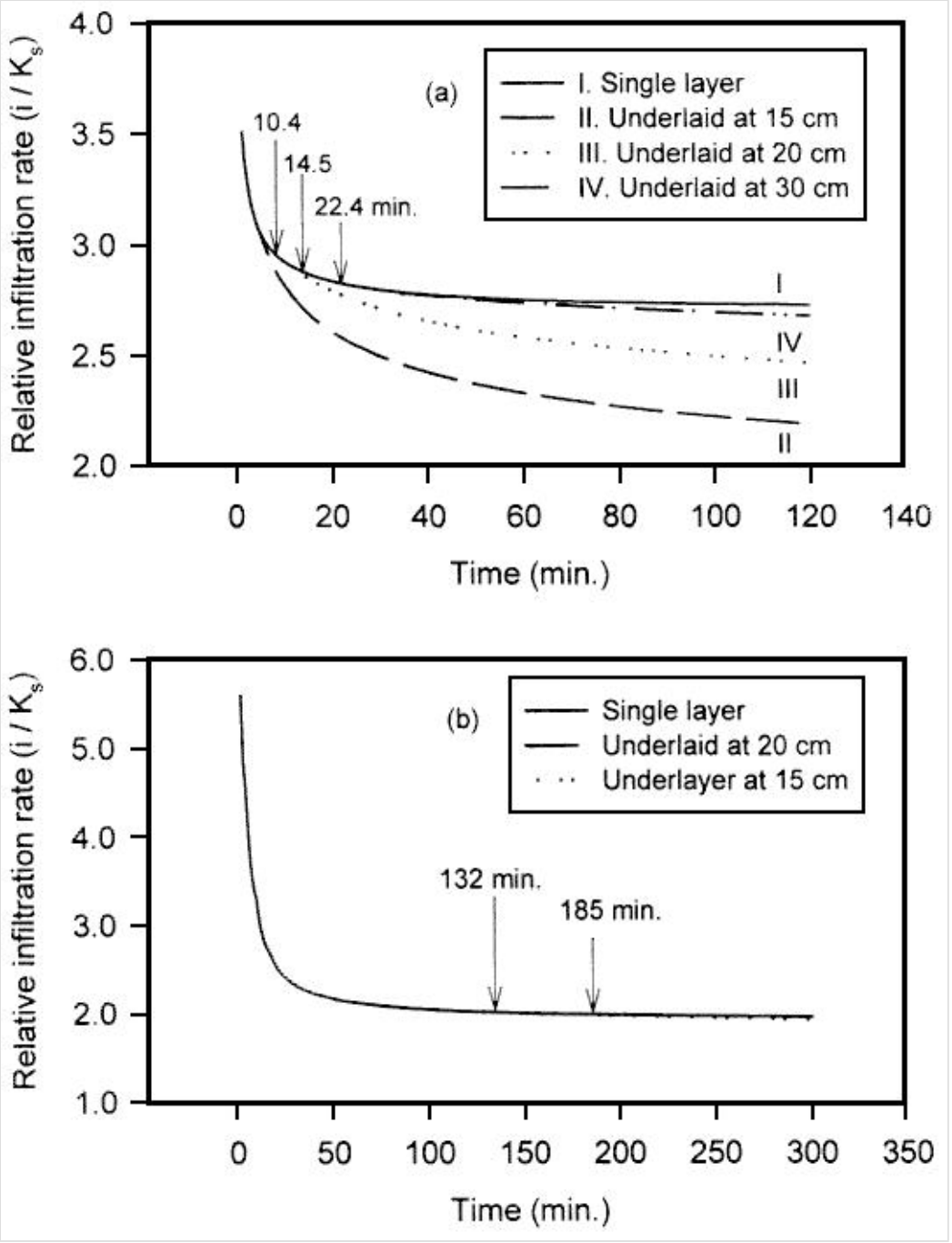

Fig. 3. Layering influence on infiltration rate during a 300-min. infiltration simulated for the sandy clay loam overlaid on Yolo light clay (a) and Berino fine sand overlaid on sandy clay loam (b). The relative position of the wetting front and texture discontinuity affect the measured infiltration rates.

The difference in *i* between the uniform soil profile and layered soil appears to be time dependent. Before the wetting front reaches the interlayer, the infiltration rate is the same for both the uniform and for the layered soil. Thus, if the measurement is short enough, no difference will be observed, whereas if the measurement lasts long enough, the difference will become more pronounced. Long infiltration times may be necessary for quantifying management practices where prolonged irrigation times are used. Because single-ring infiltration rates can be reasonably well scaled to 1-D infiltration rates using the *f* factor, the depth of infiltration (wetting front position), where $d_{wf}(t)$ can be estimated by Equation (10) where $[theta]_i$ is initial soil water content. The estimated times for the wetting front to reach 15, 20, and 30 cm in the Berino fine sand were 10.5, 14.0, and 22.5 min., and to reach 15 and 20 cm in the sandy clay loam, they were 132 and 185 min. The estimated times (arrows in Fig. 3) to reach the respective interfaces of the texture discontinuity for the cases of the sandy clay loam overlaid on the Yolo light clay (Fig. 3a) and the Berino fine sand overlaid on the sandy clay loam (Fig. 3b) were both close to those times that showed departure of simulated infiltration rate in layered soil from the infiltration rate in a uniform soil.

$$d_{wf}(t) = \frac{1}{(\theta_s - \theta_i) f} \int_0^t i(t)\,dt$$

Equation 10

CONCLUSIONS

Numerical simulation showed that vertical infiltration rate (1-D infiltration) and single-ring infiltrometer were different by a correction factor of *f.* The *f* values are related to soil hydraulic properties, initial and boundary conditions, and the ring geometry. In practice, it is important to remember that infiltration rate is time dependent when different ring configuration and initial and boundary conditions are used.

For a fine soil, constant and falling head methods produce very similar infiltration rates for a time period practical for field measurement (e.g., a few hours) because the head drop in the ring is small. However, for a coarse textured soil, the head drop is fast. Thus, the falling head method measures substantially lower infiltration rates if the measurement is taken when the ponded head is small. Measurements taken immediately after refilling the infiltrometer will be close to the infiltration rate by the constant head method.

The effect of layering on infiltration measurement is time and position dependent. For a limited period of measurement, the layering effect is more profound when the underlaid soil is closer to the surface. The time required for the wetting front to reach the interface of texture discontinuity can be estimated from the correction factor, *f,* and the cumulative infiltration.

REFERENCES

Bouwer, H. 1960. A study of final infiltration rates from cylinder infiltrometers and irrigation furrows with an electrical resistance network. 7th International Congress of Soil Science, Madison, WI. [Context Link]

Bouwer, H. 1963. Theoretical effect of unequal water levels on the infiltration rate determined with buffered cylinder infiltrometers. J. Hydrol. 1:29-34. [Context Link]

Bouwer, H. 1986. Intake rate: Cylinder infiltrometer. *In* Methods of soil analysis, Part 1, 2nd Ed. Agron. Monog. 9. ASA and SSSA, Madison, WI. A. Klute (ed.). p. 825-844. [Context Link]

Elrick, D. E., G. W. Parkin, W. D. Reynolds, and D. J. Fallow. 1995. Analysis of early-time and steady state single-ring infiltration under falling head conditions. Water Resour. Res. 31:1883-1893. [Context Link]

Elrick, D. E., W. D. Reynolds, H. R. Geering, and K. Tan. 1990. Estimating steady infiltration rate times for infiltrometers and permeameters. Water Resour. Res. 26:759-769. [Context Link]

Fallow, D. J., and D. E. Elrick. 1996. Field measurement of air-entry and water-entry soil water pressure heads. Soil Sci. Soc. Am. J. 60:1036-1039. [Context Link]

Hanks, R. J., and S. A. Bowers. 1963. Influence in variation in the diffusivity-water content relation on infiltration. Soil Sci. Soc. Am. Proc. 27:263-265. [Context Link]

Hillel, D., and D. E. Elrick (eds.). 1990. Scaling in soil physics: Principles and applications. SSSA Spec. Publ. 25, SSSA, Madison, WI.

Hills, R. G., I. Porro, D. B. Hudson, and P. J. Wierenga. 1989. Modeling one-dimensional infiltration into very dry soils. 1. Model development and evaluation. Water Resour. Res. 25:1259-1269. [Context Link]

Pan, L., and P. J. Wierenga. 1995. A transformed pressure head-based approach to solve Richards' equation for variably saturated soils. Water Resour. Res. 31:925-931. [Context Link]

Pan, L., and P.J. Wierenga. 1997. Techniques for improving numerical modeling of 2-D water flow in variably saturated and heterogeneous porous media. Soil Sci. Soc. Am. J. 61:335-346. [Context Link]

Philip, J. R. 1966. Absorption and infiltration in two- and three-dimensional systems. *In* Water in the unsaturated zone. P. E. Rijtema and H. Wassink (eds.). UNESCO, Paris, pp. 503-525. [Context Link]

Philip, J. R. 1969. Theory of infiltration. Adv. Hydrosci. 5:215-296. [Context Link]

Reynolds, W. D., and D. E. Elrick. 1990. Ponded infiltration from a single ring: I. Analysis of steady state flow. Soil Sci. Soc. Am. J. 54:1233-1241. [Context Link]

Tricker, A. S. 1978. The infiltration cylinder: Some comments on it's use. J. Hydrol. 36:383-391. [Context Link]

van Genuchten, M. Th. 1980. A closed-form equation for predicting the hydraulic conductivity of unsaturated soils. Soil Sci. Soc. Am. J. 44:892-898. [Context Link]

Warrick, A. W., D. O. Lomen, and S. R. Yates. 1985. A generalized solution to infiltration. Soil Sci. Soc. Am. J. 49:34-38. [Context Link]

Wu, L., and L. Pan. 1997. A generalized solution to infiltration of single-ring infiltrometers. Soil Sci. Soc. Am. J. 61:1318-1322. [Context Link]

IMAGE GALLERY

Select All Export Selected to PowerPoint

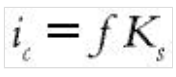
Equation 1

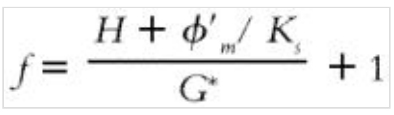
Equation 2

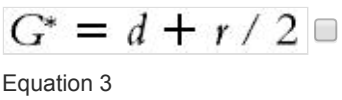
Equation 3

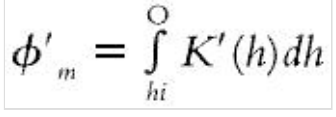

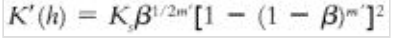
Equation 5

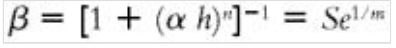
Equation 6

Equation 4

$$Q_t = (\pi / G)(K_{fs}H(t) + \phi'_m) + \pi r^2 K_{fs}$$

Equation 7

$$H(t) = (H_0 + \phi'_m / K_{fs} + \pi rG)\exp(-rK_{fs}t/\pi r^2 G) - \phi'_m / K_{fs} - \pi rG$$

Equation 8

$$G = 0.316(d / r) + 0.184$$

Equation 9

Table 1

Table 2

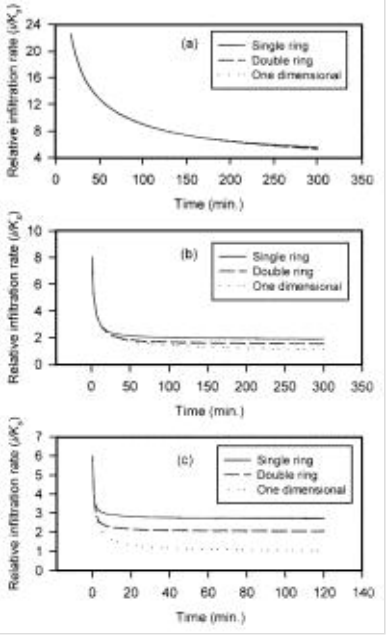

Fig. 1

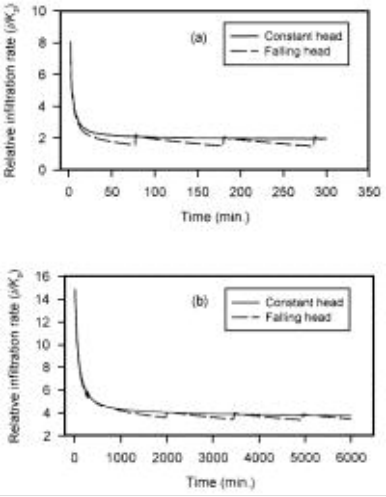

Fig. 2

Table 3

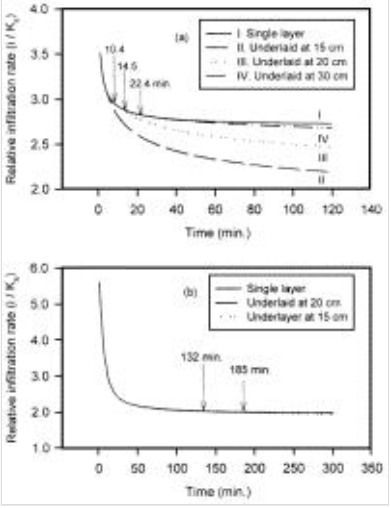

Fig. 3

$$d_{wf}(t) = \frac{1}{(\theta_s - \theta_i) f} \int_0^t i(t)dt$$

Equation 10

Back to Top